İSTANBUL UNIVERSITY
CERRAHPAŞA

RESEARCH ARTICLE
Electrica 2021; 21(2): 189-202

Force-Sensitive Classic Toothbrush: System Analysis, Design, and Simulation

Md Akhtaruzzaman

Department of Computer Science and Engineering, Military Institute of Science and Technology, Mirpur Cantonment, Dhaka, Bangladesh

Cite this article as: M. Akhtaruzzaman, "Force-Sensitive Classic Toothbrush: System Analysis, Design, and Simulation", Electrica, vol. 21, no. 2, pp. 189-202, May, 2021.

ABSTRACT

Starting from the chewing stick to the smart toothbrush, methods of brushing the teeth in the elite society have improved greatly. But so far, the usage of manual toothbrushes is much higher than that of the automatic ones. Brushing is an everyday practice; it is very important to ensure a constant, applied force in the range of 1.0-2.5 Newtons, and duration should be 2-4 minutes. Excessive pressure on the teeth will damage the gums and enamels. Conversely, insufficient pressure and shorter duration will not serve the purpose of brushing. Brushing teeth with a classic toothbrush results in uncertainty in terms of applied pressure and duration. Thus, improvement in the general design of the classic toothbrush is necessary. This paper presents the design of a force-sensitive classic toothbrush which will ensure the pressure applied during brushing is in between a certain minimum and maximum. The classic toothbrush with a smart sensing capability will enhance the brushing exercise and make it more efficient and effective. A tiny circuit was designed for sensing, decision making, and indication of applied forces. The system was modeled using simulations, and a prototype was developed. The prototype was tested with several weights (50 g–300 g). The results show the viability of the proposed system for practical applications in the general market.

Keywords: Toothbrush, classic toothbrush, force-sensitive toothbrush, smart toothbrush, pressure sensitive toothbrush

Introduction

Outcomes of brushing the teeth depend on the type of toothbrush and the individual's dexterity, habit, skills, knowledge, attitude, agility, and usage frequency. A good brushing habit influences the effectiveness of brushing the teeth [1]. The evolution of the toothbrush presents various forms from the Chew-stick through Hog's hair and Nylon bristle classic toothbrush to the modern automatic brushes [2]. Studies have shown that a steady force and time duration are very important to get proper results from brushing. Too much pressure on the teeth will damage the enamel and gums. On the other hand, less pressure will defeat the purpose of brushing the teeth in terms of cleanliness and gum care. Maintaining the right pressure is difficult while using classic (manual) toothbrushes, thus it needs to be improved in design and function.

Classic toothbrushes are more popular than the automatic ones because of the lower unit price and lower maintenance cost. Considering the high demand, the design of the manual toothbrush needs to be improved through a mechatronics design strategy in such a way that the basic structure of the classic (manual) toothbrush does not change but upgrades to its next level. Retaining the basic structure and low-cost will maintain the popularity of classic toothbrushes, and at the same time, mechatronics system design will make the device smarter.

Recent statistics have shown that the usage of manual toothbrushes in the USA is about 4.7 times higher than that of the powered toothbrushes (usage: manual toothbrush >80%; powered toothbrush ≈17.43%) [3, 4]. The trend of using toothbrushes in the USA (presented in Figures 1 and 2) shows that in 2011, 39.89 million people (≈12.80%) were using automatic toothbrushes which increased to about 17.43% (57.56 million) in 2019 and is predicted to be approximately 18.14% (≈ 61.78 million) in 2023 [4].

Corresponding Author:
Md Akhtaruzzaman

E-mail:
akhter900@gmail.com;
akhter900@cse.mist.ac.bd

Received: January 19, 2021

Accepted: April 20, 2021

DOI: 10.5152/electrica.2021.21007

Content of this journal is licensed under a Creative Commons Attribution-NonCommercial 4.0 International License.

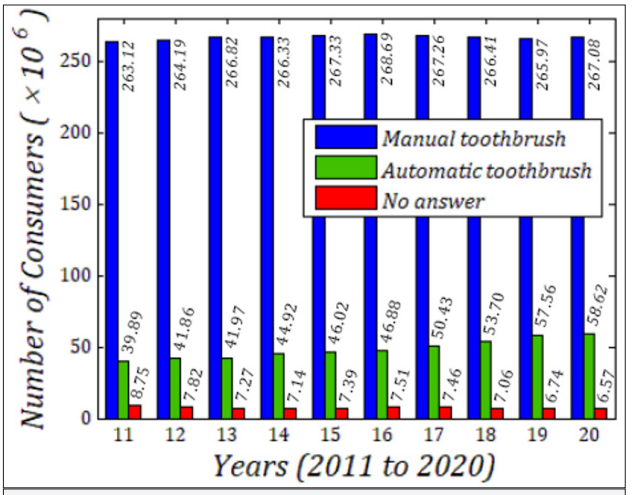


Figure 1. Usage of toothbrushes in the USA, year 2011 to 2020

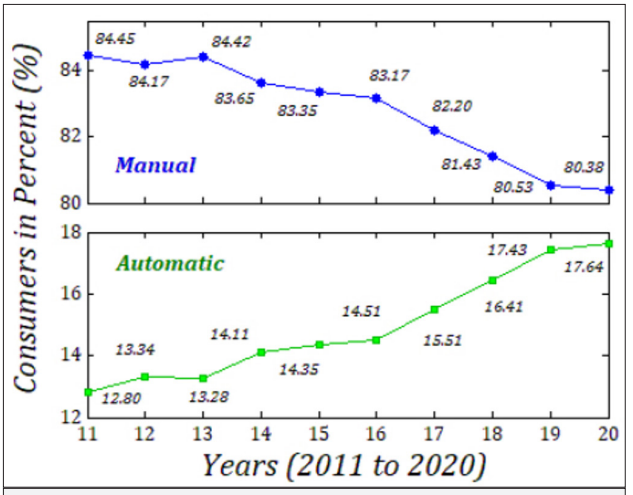


Figure 2. Percentage (%) usage of toothbrushes in the USA, year 2011 to 2020

Although the usage of powered toothbrushes in the USA is increasing, the use of manual toothbrushes is much higher (mean value ≈82.14%) compared to the use of powered toothbrushes (mean value ≈15.65%). Although, the use of manual toothbrushes is decreasing in percentage (Figure 2) terms, it is increasing in terms of numbers as reflected in Figure 1; in the year 2011, there were ≈263.12 million users of manual toothbrushes which increased to ≈265.97 million in 2019, and the number is projected to be higher (≈272.25 million) in the year 2023.

Statistics of toothbrush use in UK from 2015 to 2018 show almost the same characteristics. The usage of electric toothbrushes is increasing while the use of the standard toothbrush is decreasing [5]. But the use of manual toothbrushes in the UK is more (≈59.00%) [6]. The emerging markets for toothbrushes (2014) in Germany, Italy, Japan, France, and Russia have shown significant growth in the automatic toothbrush market. But this growth cannot compete with the market for manual toothbrushes as the latter is more than 50% of total market value [7].



Figure 3. Various types of toothbrushes currently available in the market

Very few studies were found on the usage of toothbrushes in the Asian region, especially in Bangladesh. A recent study has shown that the brushing habits of the Bangladeshi people are very poor and inefficient; about 25.45% people use toothbrushes (mostly classic ones), about use chewing sticks, and about people still are in the habit of using fingers to clean their teeth [8]. The emerging market for toothbrushes in 2014 also showed the maximum sale of manual toothbrushes in Brazil, Indonesia, Vietnam, and India [7]. One of the important reasons behind the popularity of manual toothbrushes is lower unit price and maintenance cost. Statistics show that the automatic toothbrush unit cost, replacement head cost, and replacement (once in every three months) cost per year are about 55$, 10$, and 40$, respectively. The manual toothbrush unit and use (replace every 3 months) costs are about 1-2$ and 4-8$, respectively [7].

As the uses of manual toothbrushes are more, design of manual toothbrushes is being refined and modified with a variety of styles, shapes, and sizes in handles, heads, and bristles to make the classic toothbrushes more effective in improving oral health and plaque removal. Beside this classic toothbrush, several advancements of toothbrush technology are found these days, for example: Silicon, Silicon hybrid, Baby finger, Triple bristle, Rotary head, Vibrating head, Amabrush, and Encompass. Various types of commercially available toothbrushes are shown in Figure 3.

Though, both classic and automatic toothbrushes have some pros and cons, in most of the cases they have shown similar results in maintaining oral health [9-11]. Design of automatic toothbrushes must be well engineered (Mechatronics engineering approach: merging Mechanical, Electrical-electronics, and Artificial intelligence (AI) in one discipline) to ensure safety. Comparisons between classic and powered toothbrushes in terms of usage, functionality, safety, and objectives are presented in Table 1 [2, 9-13].

Table 1. Comparison between Classic and Electric Toothbrushes [2, 9-13]

Focus Points	**Manual Toothbrush**	**Electric Toothbrush**
Unit price	very Low	High
Maintenance	Very Low	High
Usages	High	Medium
Activity/control	Self/Manual	Powered
Portability	Easy	Comparatively complex
Rotation/vibration frequency	Very low	Variable frequencies
Indication/Alert	No	Available
Interactive	No	Yes
Comfortability	Self-controlled	Yes
Feedback to user	No	Yes (mostly)
Data recording	No	Yes (mostly)
Replacement	With new toothbrush (mostly)	Only brush head (mostly)
Time tracking	No	Yes (mostly)
Pressure tracking	No	Sometimes
Loosen plaque	Yes (depending on uses behavior)	Yes (comparatively effective)
Gum care	Depends on brushing habits	Comparatively effective
Reducing gingivitis risk	Depends on brushing habits	More effective for both short-term and long-term use
People with arthritis and limited dexterity	Cannot use (very difficult to use)	Comparatively easy to use
Toothpaste usage quantity	0.3 to 2.1 gram	0.2 to 1.2 gram
Fluoride concentration in saliva	After brushing no significant differences in "Fluoride vs Time" graphs for both cases	
Safety in terms of secondary injury	Safer (self-controlled)	Must ensure safety (machine-controlled)
Sustainable development	No	No
Recycling	Comparatively easy	Comparatively complex

There are some potential opportunities for improving the style of manual toothbrushes, both by design and AI. The earlier stages of current research developed a prototype of a smart classic toothbrush where Arduino-Nano µ-controller was used for sensing pressure feedback, taking decisions, and producing outputs through indicator LEDs [2]. Use of the Arduino-Nano µ-controller for this job results in a huge waste of memory and processing power; rather, the µ-controller is suitable for complex systems like robots, complex mechatronics systems, or complex control [14, 15]. A dedicated tiny circuit may solve this problem with improved styles and reduction in production cost. Sustainable development in the design of manual (classic) smart toothbrushes is obligatory and must be taken into consideration by the researchers [16].

About 90% of dental and gum diseases are caused because of inefficient and incorrect brushing practice [8]. Though the recommended time for brushing teeth is 2 to 4 minutes (120 to 240 seconds), the average time of brushing is about 1 minute (60 seconds) [8, 12, 13]. The main reasons for inefficient brushing are poor knowledge, incognizance, tiredness, discomfort, inefficient brushing, damaged or inefficient design of bristle, dexterity, sensitivity, no tracking of time or pressure, and choice of wrong toothbrushes. Maintaining appropriate pressure is another important factor for good dental health [2, 13]. One of the main causes of tissue abrasion and damage to teeth substance is excessive pressure while applying bristles on teeth [2, 17]. Different researchers have used and suggested various ranges of applied pressure for brushing teeth.

Table 2. Pressure ranges for brushing

Literatures	Research Focus	Min Pressure (g)	Max Pressure (g)
Giuliani, McMahon and McInnes [17]	Design of a toothbrush with adaptive load sensor	30	150
Slocum and Slocum [18]	Design of force sensitive toothbrush with bi-stable mechanism into the toothbrush handle.	50	250
Bizhang et al. [19]	In Vitro Study: Influence of Bristle stiffness of Manual Toothbrushes	≈50	300
Matsumoto and Musha [20]	Design of an instrument to detect precise toothbrushing pressure	150	250
Dirksing [21]	Design of force-indicating toothbrush with magnetic latching	150	300
Spieler and Berman [22]	Design of a force sensitive toothbrush handle with indication of variation of applied force	200	300
Chiyoda [23]	Design of a toothbrush with polishing pressure sensor	≈50	300
Miller [24]	Designing a Hall-effect based pressure sensing powered toothbrush	≈50	300
	Average value	≈91	≈268
	Predicted range	100	250
	Considerable range	102 (1.0N)	255 (2.5N)

Giuliani et al. [17] presented a toothbrush with an adaptive load sensor and suggested an applied pressure range of 30 to 150 g. Another research conducted by Slocum and Slocum [18] presented the mechanical design of a force-sensitive toothbrush in which the applied pressure on the bristles was in the range of 50 to 250 g [18]. A maximum pressure of 300 g for brushing was considered in another experiment conducted by Bizhang et al. [19]. On the basis of the literature reviews, the accepted range of applied pressure for brushing teeth can be considered as ≈100 to ≈250 g. Various pressure ranges suggested in various literatures are presented in Table 2.

This article presents the prototype design of a novel smart toothbrush, which can be used like as classic toothbrush, while having a sense of the applied force while brushing. The limits of the acceptable applied forces are indicated through two color LEDs. This will improve the brushing experience by preventing damage to gums and enamel.

System Design

The proposed prototype is designed to determine the feasibility of the force-sensitive toothbrush for general use. A Force Sensitive Resistor (FSR) is the key sensor element in the prototype. The FSR is placed just beneath the bristles to get a feedback of the pressure applied on teeth by the bristles. This is a big challenge in designing the prototype. Another challenge is to make the brush waterproof so that fluids like water or saliva cannot ruin the internal electrical connectivity. For the design of the prototype, water proofing was not considered as experiments were not conducted on real subjects. The prototype proves the applicability of the proposed system.

Physical design of the prototype

The prototype is based on the structure of a manual toothbrush available in the local market. The head of the toothbrush is cut into two layers very carefully so that the bottom layer does not lose its strength and bristles at the top layer do not lose their attachment. This layer cut is continued till the brush neck to achieve enough flexibility of the top layer so that the induced pressure can be transmitted to the middle layer. The FSR sensor is placed in the middle layer with a brush-head shaped jacket made of an elastic material. For this prototype, a double sided, Pressure Sensitive Adhesive (PSA) tape was used (3M VHB PSA 4949). Two conducting wires were soldered to the two pins of the FSR sensor and carefully taken out at the neck of the toothbrush. The placement of sensor layer, just beneath the bristle area, is shown in Figure 4.

At the brush handle, two slots are cut to fit a custom designed, small-sized circuit-board and three button-cell batteries (shown in Figure 5). For safety, a tiny switch is also mounted at the brush-handle. Two LEDs (Green and Red) are attached at the back side of brush-neck. The circuit is designed to indicate three levels of applied pressure: (a) if force is below 100, no indication through LEDs; (b) if the applied force is in between 100 to 250, the Green LED will turn on; and c) the Red LED will be turned on if the applied force exceeds 250 g, indicating a potential threat of teeth damage.

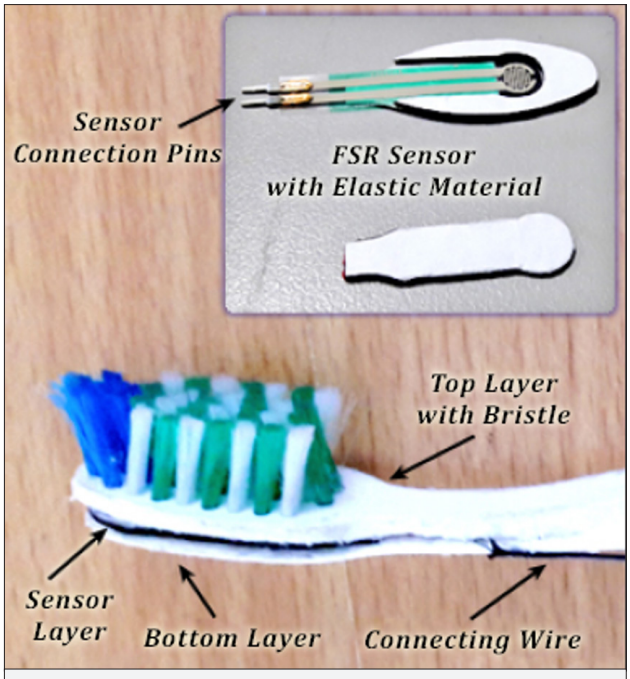


Figure 4. Placement of sensor layer beneath the bristle

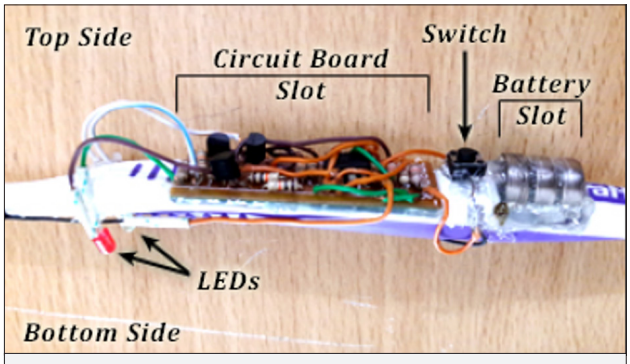


Figure 5. Toothbrush handle with necessary components

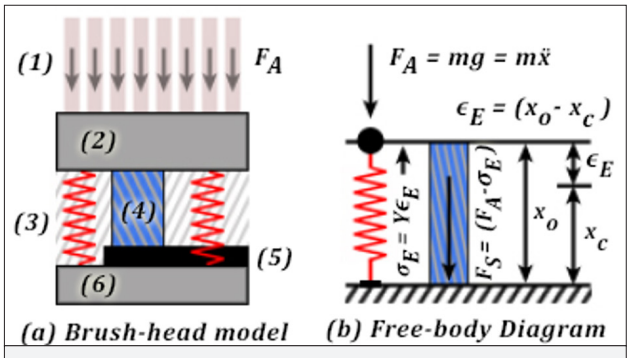


Figure 6. a, b. Mass-spring model of the elastic material; (a) brush head model where (1) is the applied force F_A, (2) is the bristle attachment layer, (3) is the elastic layer, (4) is the non-elastic material at the top of the sensor head, (5) is the sensor body, (6) is the bottom layer of the brush head; and (b) simplified model of the brush head.

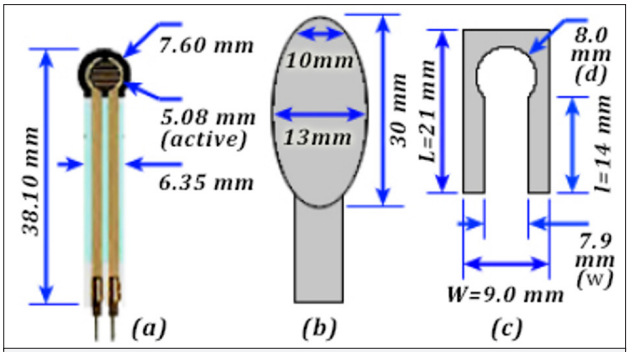


Figure 7. a-c. Determination of the total area of the elastic material where pressure (force on bristle) is applied; (a) FSR 400 sensor module sizing, (b) inner surface area (elastic material) of brush head, and (c) simplified surface of the elastic material

System Modeling

The proposed smart toothbrush is modeled based on the elastic material used as the intermediate layer where the FSR sensor is integrated. Depending on the elasticity of the material, the sensing of the applied force is adjusted. To determine the actual induced force on the FSR, Eq. (1) is used were F_S is the force induced on the FSR which is the residual of the total applied force (F_A) on the surface area of the elastic material and the reaction force (σ_E) of the elastic material. The total reaction force (σ_E) of the elastic material is calculated by multiplying the total area (A_U) and unit reaction force ($\gamma\varepsilon_E$), where γ is the Young's modulus of the elastic material and ε_E is the strain per unit area, presented in Eq. (2). The brush-head mass-spring model and the corresponding free-body diagram are presented in Figure 6. To calculate the active surface area of the elastic material, a simplified model of the surface is presented in Figure 7. The active area is calculated using Eq. (3).

$$F_S = F_A - \sigma_E \tag{1}$$

$$\sigma_E = A_U\gamma\varepsilon_E = A_U\gamma(x_0 - x_c) \tag{2}$$

$$A_u = (L \times W) - \left(\frac{\pi d^2}{4} + (l \times w)\right) \tag{3}$$

To model the applied force on the sensor head, in Figures 6 and 7, some factors are considered as negligible and thus ignored. These factors are, damping coefficient of the elastic material, some area-intersection, and surface overlapping. The value of Young's modulus in Eq. (1) was identified as 5×10^2 *kPa* ≈ 0.5*N. mm*$^{-2}$ from the data sheet of 3M VHB Acrylic PSA Foam Tape, 4949 [25, 26].

Research has presented strain-stress characteristics of pressure loaded foam material based on Mass-spring or Mass-spring-damper modeling [27, 28]. The rigid polyurethane foam (288 kg/m^3 & 50 × 50 × 50 mm^3) model was presented by Mane et al. [28] in which three regions are observed in the strain-stress characteristic graph. The first region shows linear elastic behavior for small strains (5.0%–10.0%) reflecting the Young's modulus of the foam material. The same characteristics were also presented by Goga and Hučko [29] in their compressive strain-

stress model of polyurethane and aluminum foam solids (50 × 50 × 50 mm^3) of various densities. The characteristics of elastic material show that higher density increases the impedance of the material in terms of compressive resistance, thus increase of the Young's modulus presents less elasticity of the material.

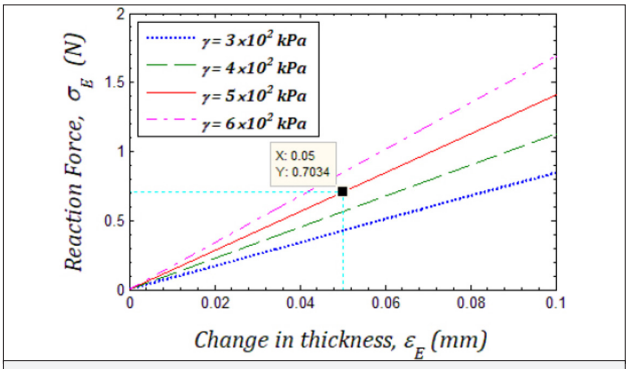


Figure 8. Mass-spring model response (ε_E *vs.* σ_E graph) of the linear elastic region for ≈ 10% compression of the 3M VHB PSA 4949 Foam (thickness = 1.1 mm) and determination of the total reaction force σ_E=0.7034N at compressive deformation ε_E=0.05 mm

Table 3. Mechanical Specification of 3M VHB PSA 4949 Acrylic Foam Tape [25, 26, 31]

Property	Values
Type	Acrylic Foam Closed Cell
Thickness	1.1 *mm*
Density	800.0 *kg.m*$^{-3}$
Elasticity modulus (γ)	510^2 *kPa* ≈ 0.5 *N.mm*$^{-2}$
Linear elastic behavior	5 - 10% Compression
Color	Black
Contact surface at the inner layer	202.44 mm^2

Table 4. Specification of FSR 400 sensor [30]

Property	Values
Type	FSR 400 (Interlink Electronics)
Length	38.10 mm
Tail width	6.35 mm
Head diameter	7.60 mm
Nominal Thickness	0.30 *mm* (Adhesive layer: 0.05 *mm*; Conductive layer: 0.10 *mm*; Spacer layer: 0.05 *mm*; Semiconductive layer: 0.10 mm)
Active area diameter	5.08 mm
Switch travel	0.05 mm
Force sensitivity	≈ 0.2-20.0N
Stand-off resistance	>>10^7 Ω

In this research experiment, the mass-spring model was adopted for elastic material (PSA) used at the middle layer. Total contact area of the PSA at the brush head was calculated as A_U=28.1345 mm^2. As the FSR sensor-head spacer thickness (switch travel) was 0.05 mm [30], the compression of PSA would be 0.05 mm, creating a reaction force σ_E. Other than this, the deformation of the sensor material was considered negligible. The simulated graph of the model is presented in Figure 8 where the reaction force is determined to be about 0.70 *N* for 0.05 mm compressive deformation of the PSA material. Thus, the residual force applied on the sensor is in the range of 0.3 *N* (30.61 g) to 1.8 *N* (183.67 g) where the actual applied force on the bristle is 0.98 *N* (100 g) to 2.45 *N* (250 g). Necessary parameter specifications are presented in Table 3 (3M VHB PSA 4949 Foam) and in Table 4 (FSR 400) [25, 26, 30, 31].

Circuit Analysis and Design

The stand-off resistance of FSR is >107Ω (theoretically $R_{FSR} \rightarrow \infty$ in the normal condition). The resistance decreases depending on the applied (increasing) pressure on the FSR sensor. Thus, a potential divider circuit can be designed to determine the change in voltage (V_O) with the change in resistance. This variation of voltage is compared with two reference voltages (V_{Ref1} and V_{Ref2}), which are basically the range (lower and upper limits) of voltages for the change in FSR resistance against the applied acceptable pressure values. The output of the two comparators connects to the Green and Red LEDs. The Green LED turns on if the voltage (V_O) stays in between the two reference voltages, and red LED turns on if the voltage (V_O) crosses the highest reference (V_{Ref2}) value. Only one LED turns on for a particular time.

Considering the potential divider circuit, if no pressure is applied on the sensor, V_{Ref1} (V_O) can be measured as 0 (zero). Depending on the applied increasing pressure, the resistance of FSR decreases, and V_O increases, which can be determined by Eq. (4) if the value of the variable resistor (R_{VR1}) is known. To calibrate the FSR sensor, the Force vs. Resistance (F-Ω) characteristics graph was plotted (Figure 9) through experimental investigation. The acceptable range of FSR resistance was determined (80.59Ω to 13.24Ω) from the graph. For designing the circuit, a logic table was adopted as presented in Table 5. The schematic of the proposed circuit is presented in Figure 10. In Eq. (4), R_{FSR}, R_{VR1}, V_S, *and* V_O indicate the resistance of FSR, variable resistor 1, Source voltage, and output voltage of the divider circuit, respectively.

$$V_O = \left(\frac{R_{VR1}}{R_{FSR} + R_{VR1}}\right) V_S \quad (4)$$

To ensure the two reference voltage levels, a 2nd potential divider circuit was designed with two outputs, V_{Ref1} and V_{Ref2}. Figure 11 shows the schematics of 1st and 2nd potential dividers included in the design of the main proposed circuit. The values of R_{VR1}, R_{VR2}, R_1, and R_2 were determined through several simulations and results analysis.

Eq. (4) that reflects the equation of the 1st divider circuit was simulated for four variations of R_{VR1}, as presented in Figure 12

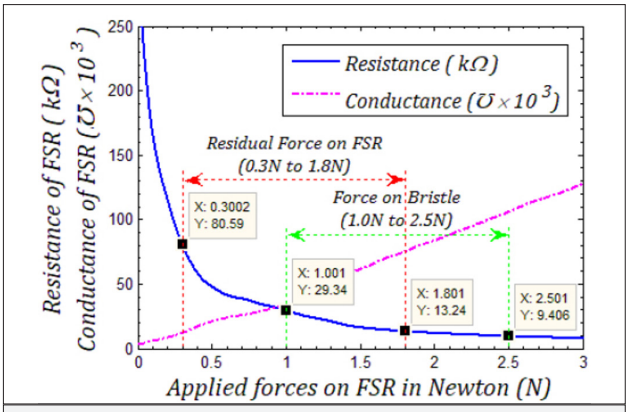


Figure 9. Force-resistance (F-Ω) and Force-conductance (F-℧) characteristics of FSR 400 (experimental results), defining the acceptable range of forces applied on the bristle and the range of the residual force

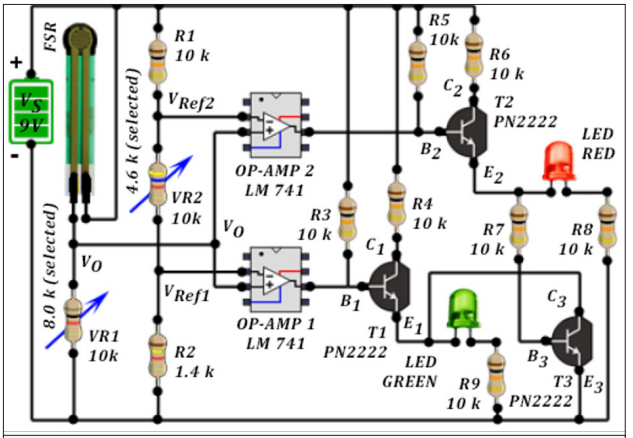


Figure 10. Circuit schematic diagram

Table 5. Logic table of the designed circuit

Force (N)	LED1 Green	LED2 Red
Low force	Low	Low
(F_A (*on bristle*) ≤1.0*N*)		
(F_S ≤ 0.3*N*)		
(R_{FSR} ≥80Ω)		
Medium force	**High**	Low
(1.0*N*≤F_A (*on bristle*)≤2.5*N*)		
(0.3*N*≤F_S≤1.8*N*)		
(80Ω≥R_{FSR}≥13Ω)		
High applied force	Low	**High**
(F_A (on bristle)≥2.5*N*)		
(F_S≥1.8*N*)		
(R_{FSR}≤13Ω)		

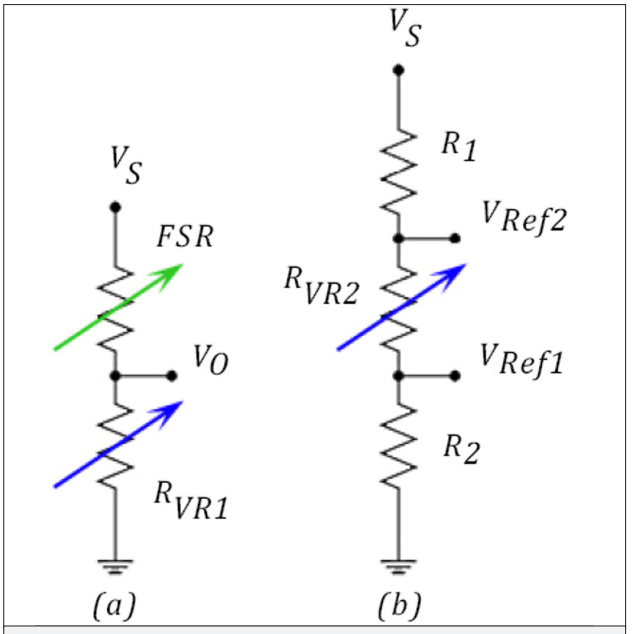


Figure 11. a, b. Potential-divider circuit schematics, (a) 1st potential-divider with FSR and R_{VR1}, and (b) 2nd potential-divider with R_1, R_2, and R_{VR2}

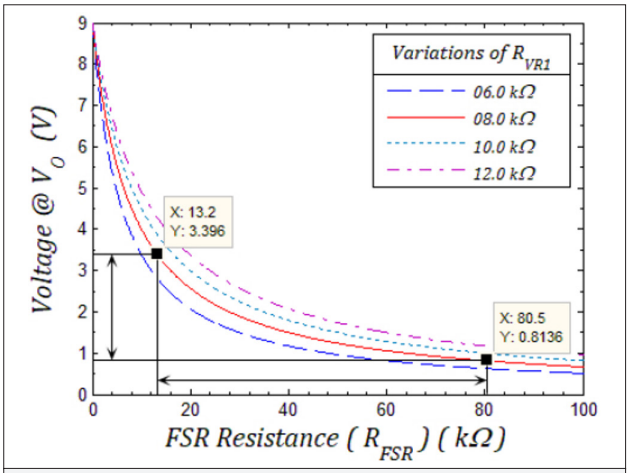


Figure 12. FSR resistance vs. Voltage (V_0) graph for variations of variable resistor 1 (one) (R_{VR1}) in the first potential-divider circuit. For R_{VR1}=08.0*k*Ω, voltage range is determined as from 0.8*V* to 3.4*V*

(R_{FSR} vs. V_0 graph). The results were analyzed based on the previously determined ranges of R_{FSR} (≈ 80.00Ω to ≈13.20Ω). From the graph, the value of R_{VR1} was selected as 8.0*k*Ω (because, 6.0 *k*Ω seemed to be small and 10 *k*Ω or 12 *k*Ω seemed to be large for the designed circuit); thus the range of voltages was determined as 0.814*V*–3.396*V*, as shown in Figure 12. This range defines the values of the two reference voltages as V_{Ref1}=0.814*V* and V_{Ref2}=3.396*V*. These indicates that (based on the logic table, Table 5), if the level of V_0 is in between the reference values (V_{Ref1}≤V_O≤V_{Ref2}), only Green LED will be turned on; if V_O>V_{Ref2}, only Red LED will be turned on. Other than this, no indication will be available.

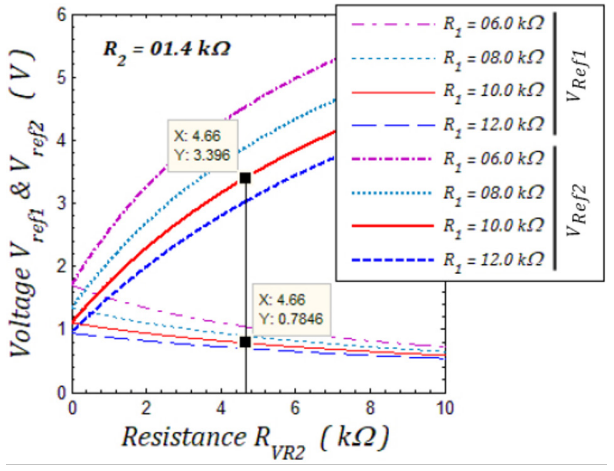


Figure 13. R_{VR2} vs. V_{Rf1} & V_{Rf2} graph to select R_1 and R_{VR2} while R_2=1.4kΩ

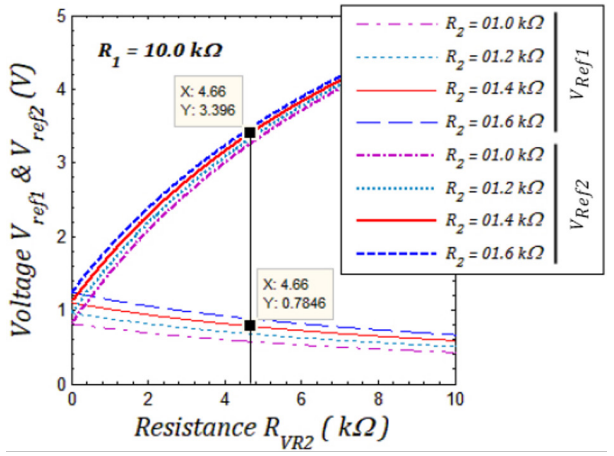


Figure 14. Determining R_2 and R_{VR2} from the characteristic graphs while R_1=10kΩ

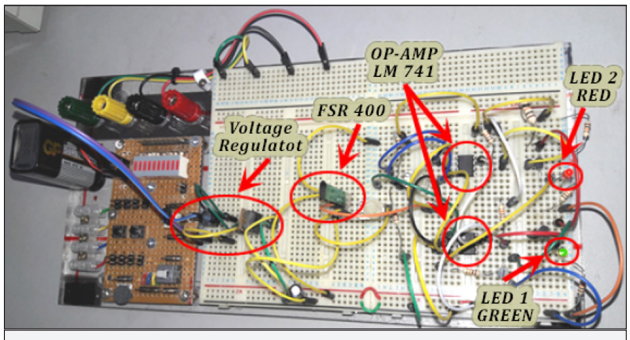


Figure 15. Preliminary test of the circuit

Selection of R_{VR1} is very important as it influences the selection of the voltage range and the proper selection of the resistors involved in the 2nd potential divider circuit (Figure 11(b)). Necessary equations (Eq. (5) and (6)) for the 2nd potential divider were simulated to observe the characteristics of the reference voltages against the variation of R_{VR2}. In Figure 13, graphs were plotted for four variations of R_1 while R_2 was fixed (R_2 = 1.4kΩ) to determine the value of R_{VR2}. It is very important to identify a single value of so that the two reference voltages (V_{Ref1} and V_{Ref2}) can be pointed out for the single value of R_1. The same theme was also verified in another simulation graph (R_{VR2} vs. V_{Ref1} & V_{Ref2}) for four different values of R_2 (presented in Figure 14) where R_1 was kept unchanged (R_1=10.00kΩ). For the experimental verification, the circuit was constructed and tested as shown in Figure 15. The selected parameters are presented in Table 6.

Table 6. Selected parameters of the proposed circuit

Components	Values
R_{VR1}	08.00kΩ
R_{VR2}	04.66kΩ (4.6kΩ)
R_2	01.46kΩ (1.5kΩ)
R_1 & R_3 to R_9	10.00kΩ
Red & Green LEDs	03.30V

$$V_{Ref1} = \left(\frac{R_2}{R_1 + R_{VR2} + R_2}\right) V_S \quad (5)$$

$$V_{Ref2} = \left(\frac{R_{VR2} + R_2}{R_1 + R_{VR2} + R_2}\right) V_S \quad (6)$$

Simulation

To observe system responses for various input patterns, the simulation of the designed circuit was performed based on the MATLAB Simulink block diagram presented in Figure 16. To simulate the change of resistance for the applied pressure on the FSR sensor, the Potentiometer block (in "*Simscape→–SimElectronics→Passive Devices*") was considered (FSR in Figure 16); it responds depending on the external signals converted into Physical Signal (PS) through Simulink-PS converter block. The sensor output (V_O) is fed to OP-AMP1 and OP-AMP2 which compare V_O with V_{Ref1} and V_{Ref2} and produce the necessary signals for the LED indicators through three NPN Transistors, NPN T1, NPN T2, and NPN T3. The resistance range of FSR Potentiometer block was set as 100kΩ and all other parameters were set based on the designed parameters from Table 6. The diagram was simulated for five different input signals, Step, Ramp, Stairs, Sine, and Triangular input signals. The amplitudes of all these input signals are in between +1 and -1 (-1 ≤ Amplitude ≤ +1). The limits of FSR resistance (0 - 100kΩ) are scaled down to 0-1 for better representation. The FSR resistance response is always the opposite of the input signal. Scope block plots output behaviors to observe, compare, and validate the system responses. In the simulated results, X-axis indicates Time (0.0 sec. to 10.0 *sec.*) and Y-axis reflects Voltage in Volts for all the graphs except the R_{FSR} that reflects the resistance of the FSR sensor.

System responses for step input signal are presented in Figure 17 where eight different signals are plotted. The first shows the

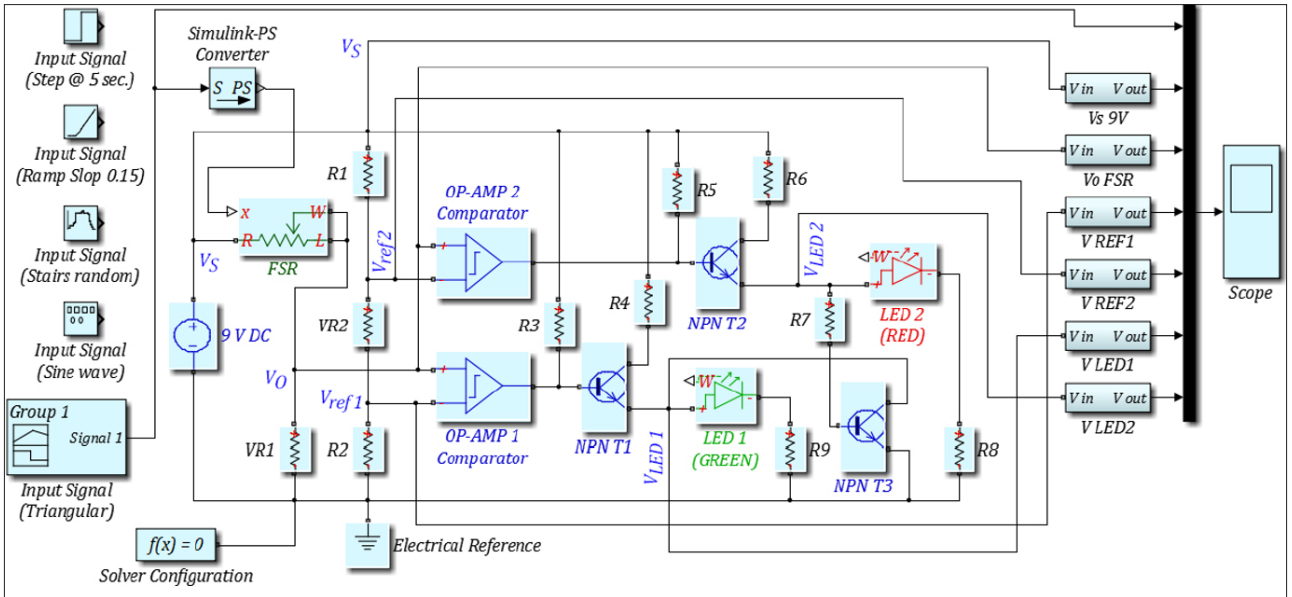


Figure 16. ForMATLAB Simulink diagram of the designed circuit to observe simulated behavior of the proposed system

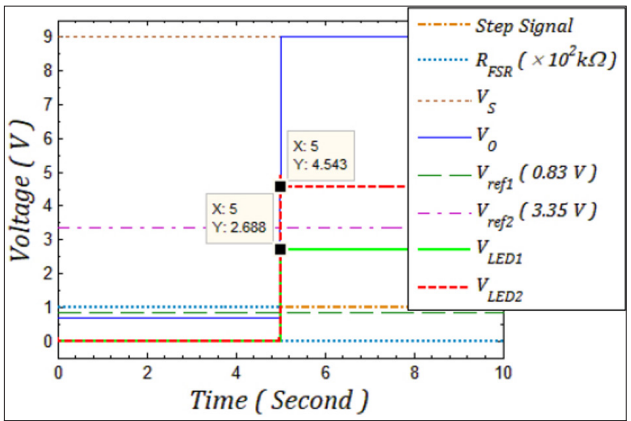


Figure 17. System responses for the step input at the 5th sec

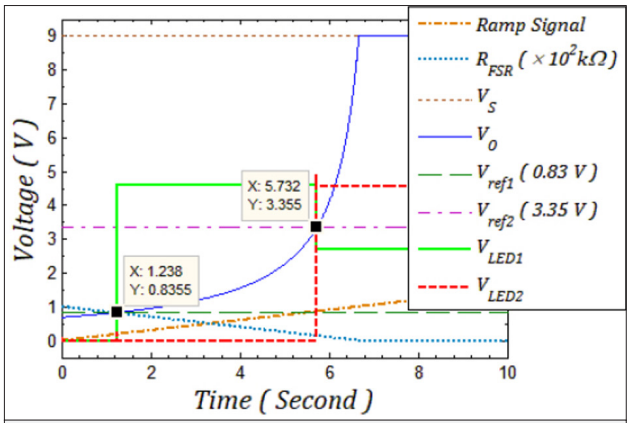


Figure 18. Ramp input (slope 0.15) response

step input signal that jumps from 0 to 1 at the 5th second. Second, the resistance of FSR that goes down from 1 to 0 at the moment of the step signal. Third, the source voltage (V_s) which is always 9*V*. Fourth, the response of V_0 that jumps from 0.69*V* to 9.0*V* at the step time. Fifth, the reference voltage V_{Ref1}=0.83*V*. Sixth, the second reference voltage V_{Ref2}=3.35*V*. Seventh, the Green LED voltage (V_{LED1}) that jumps up to the voltage level 2.688V. This voltage is lower than the LED turn-on voltage (3.3*V*); thus, the green LED status is off. Last, the voltage of the Red LED jumps up to 4.543*V* at the step time; thus, red LED status is on. The step responses of the system clarify that as the level of V_0, at the moment of the step input (5th second), crosses the level of V_{Ref2} (V_O>V_{Ref2}), the voltage at LED 2 (Red LED) becomes high enough to turn it on. Conversely, the voltage level of LED 1 (Green LED) is lower than the turn-on voltage. The level of V_0 becomes 9V at the step time because the resistance of the FSR (R_{FSR}) becomes 0.0Ω. The response satisfies the designed logic.

Simulated results for the ramp input signal are presented in Figure 18. The slope of the ramp input is considered as 0.15; thus it reaches 1.0 at ≈ 6.667 second and again reaches 1.5 at 10.00 second. With the change in input signals, R_{FSR} decreases from 1 and becomes 0 at the same time the input reaches 1. For the rest of the time, R_{FSR} remains at 0 as the resistance has reached to its lowest level. Voltage levels of V_S, V_{Ref1}, and V_{Ref2} are 9.0*V*, 0.83*V*, and 3.35*V*,respectively, as these values are always constant.

With the change in R_{FSR}, V_O increases from 0.69*V* to 9.0*V* reflecting an exponential growth pattern. V_O reaches to its highest value at ≈ 6.667second and remains unchanged. On the way to V_S, V_O intersects V_{Ref1} and V_{Ref2} at 1.238 second and 5.732 second, respectively, producing necessary activation pulses for LEDs. The voltage of LED1 (V_{LED1} for Green LED) jumps to 4.588V (Green LED is turned on) at the moment (1.238 second) V_O intersects V_{Ref1} and

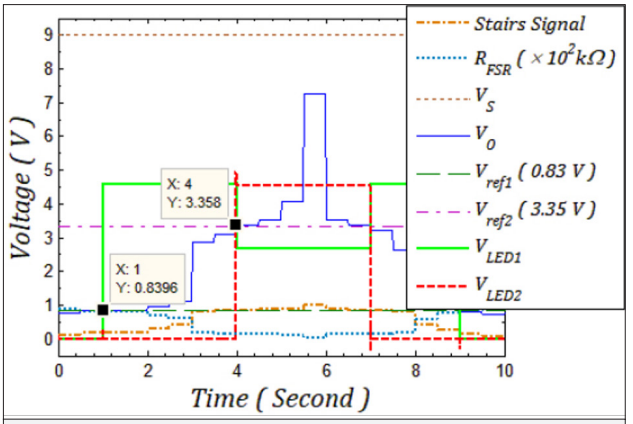


Figure 19. System responses for random stairs input

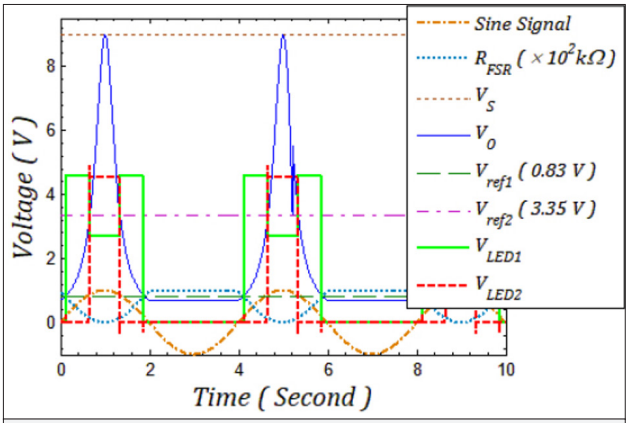


Figure 20. System response for a sine input signal

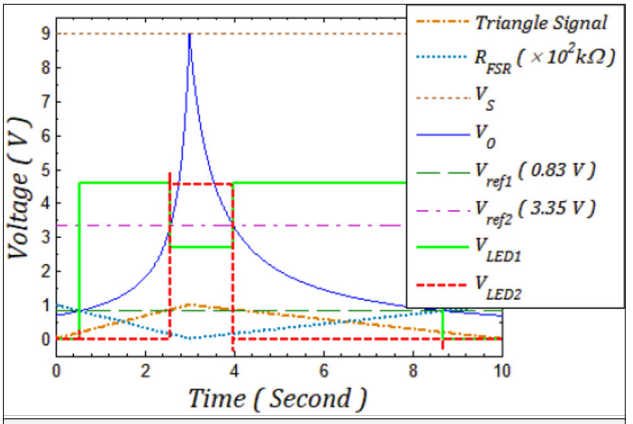


Figure 21. System responses for a Triangle input with different up and down slopes

remains unchanged till 5.732 second when V_O reaches V_{Ref2}. At this moment, the voltage level of V_{LED1} decreases to 2.688*V* turning the Green LED off and V_{LED2} becomes 4.543*V* making the Red LED on for the rest of the time. When V_{LED2} is high, the voltage level of the Green LED, V_{LED1}, does not return to level 0.0V; rather it stays at 2.688*V* which is less than the activation voltage to turn on the Green LED. The system model is also simulated for Stairs

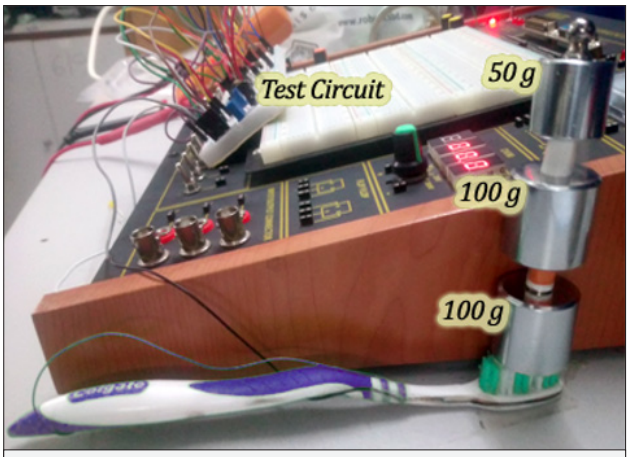


Figure 22. Experimental setup and preprototype testing

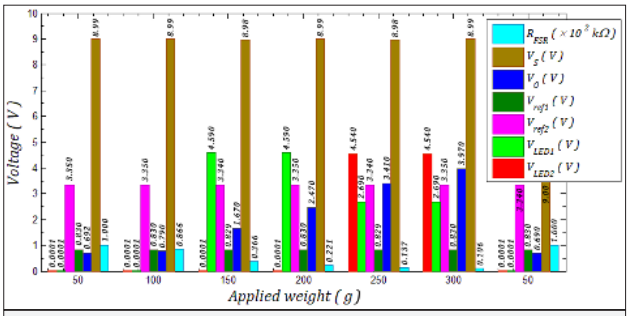


Figure 23. Experimental results with various weights applied on the bristle of the preprototype toothbrush model

input (random), Sine input, and Triangular input signals. For all the cases, system responses satisfy the designed logic. The simulated results are presented in Figures 19-21.

Experimentation and Result Analysis

After getting satisfactory results from simulations, the first stage of the system prototype was tested. The circuit was constructed on a breadboard (outside of the toothbrush) and the FSR sensor was placed beneath the bristle of a toothbrush head. The experimental setup is shown in Figure 22. The system was tested for various weights from 50 g to 300 g in steps of 50 g, directly applied by placing the weights on the bristle as shown in Figure 22. The ranges were selected based on the comparative results presented in Table 2. The step size of 50 g was chosen because of the limitations of applying weights on the bristle. Voltage levels at various nodes of the circuit were measured and recorded. The experimental results are presented in a bar diagram shown in Figure 23.

The voltages recorded during the experimentation were Source voltage (V_S), Voltage of 1st potential divider (V_O), Reference voltage one (V_{Ref1}), Reference voltage two (V_{Ref2}), Green LED voltage (V_{LED1}), and Red LED voltage (V_{LED2}). The resistance variation of the FSR in the circuit could not be measured; thus, it was calculated and scaled down to the range 0 to 1. From the experimented results it is observed that no responses (in terms

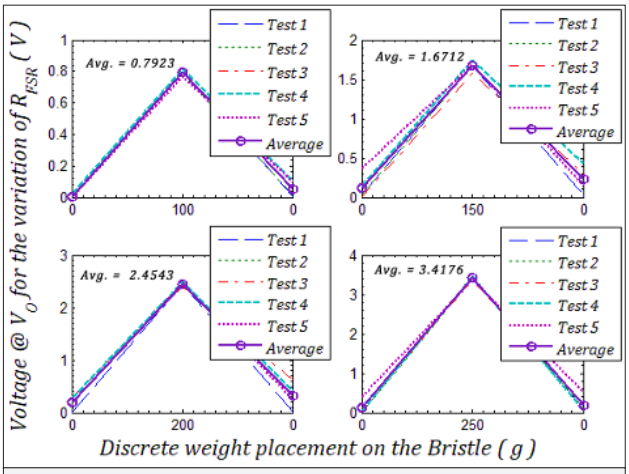


Figure 24. Triangular profile of V_0 for discrete weights on the bristle

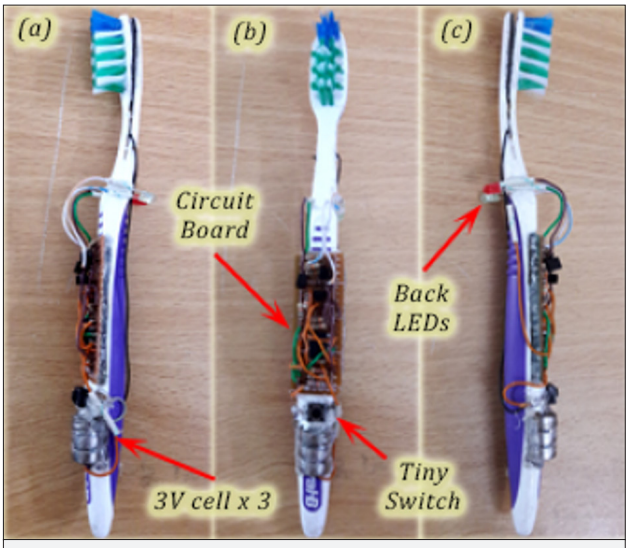


Figure 25. a-c. Prototype of smart classic toothbrush, (a) left, (b) front, and (c) right

of LED on-off) of the system are available for 50 g and 100 g. This is because, for both weights, the voltage level of V_O does not cross the reference voltage V_{Ref1}≈0.83*V*; thus, the output of the OP-AMP1 stays low and does not activate NPN T1 which is connected to LED1.

For 150 g and 200 g, voltage V_O crosses the limit of V_{Ref1} but remains lower than the 2nd reference level V_{Ref2}≈3.340. So, the +ve input becomes greater than -ve of OP-AMP1 comparator and produces an output to activate NPN T1, turning on LED1. This response is observed in the graph (Figure 23) where V_{LED1}≈4.59V for 150 g and 200 g.

When applying 250 g and 300 g, the system responded by turning on the Red LED as V_O crossed V_{Ref2}≈3.340*V*. In this condition, *+ve* inputs of both OP-AMPs become higher than that of the *-ve* inputs, thus producing outputs to activate both transistors.

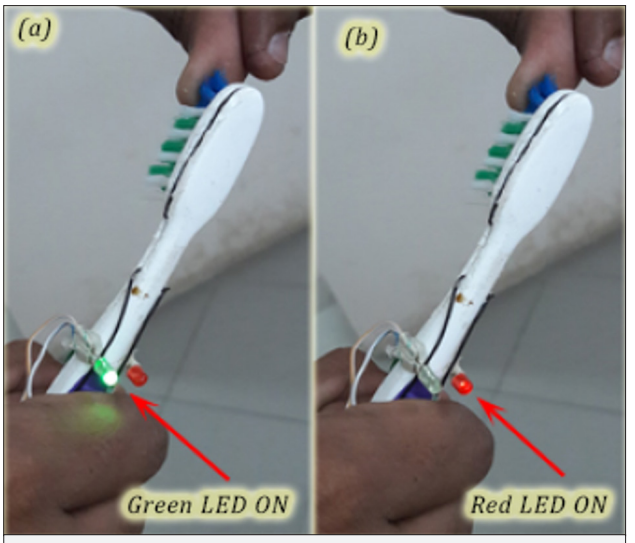


Figure 26. a, b. Prototype experimentation, (a) Green LED is on, and (b) Red LED is on.

Transistor NPN T2 allows turning on of LED2 and at the same time activates the third transistor NPN T3. Basically, this NPN T3 drains out the voltage of LED1 (emitter voltage of NPN T1) ensuring the Green LED is in off condition. The results are seen in Figure 23 for 250 g and 300 g where V_O levels are ≈ 3.41*V* and ≈ 3.97*V*, respectively, ensuring V_{LED2}≈4.54V to turn the Red LED on. At these moments, V_{LED1} stays at ≈ 2.69*V* ensuring the Green LED is off. At the end, 50 g is applied again which reflects that the responses fall back to the initial state with little variations comparing with the previous results.

The triangular profile test was also conducted for four distinct weights, reflecting the acceptable range of the applied force on the teeth while brushing. The results are shown in Figure 24. For this experiment, each weight was applied on the bristle and data were recorded for five different trials. The results show very little fluctuations with average voltages as 0.7923*V* for 100 g, 1.6712*V* for 150 g, 2.4543*V* for 200 g, and 3.4176*V* for 250 g. This validates the designed parameters.

The final experimental prototype is presented in Figure 25: (a) left view, (b) front view, and (c) right view. The prototype was tested by applying finger pressure, shown in Figure 26: (a) slight pressure that activates the Green LED, and (b) a little more pressure turns on the Red LED. For this prototype, a tiny switch was integrated with the designed circuit for safety purposes.

Conclusion

In this paper, the development of a smart classic (manual) toothbrush prototype is presented through engineering design, simulation, and experimentation. The system is conceptualized to integrate a smart mechanism with the manual toothbrush without changing its real structure. Classic toothbrushes are in high demand because of low cost and low maintenance complexity and keep a user active with full control while brushing. But in terms

of maintaining pressure and controlling aggressiveness during brushing, manual toothbrushes do not provide any feedback to the user. The applied pressure range (1.0*N* to 2.5*N* which is approximately 102 g to 255 g) is very important to prevent decay of teeth, enamel, and gums. Controlled brushing also prevents injuries. The proposed system will provide feedback on the applied pressure through indicators and will improve the brushing habit with a manual toothbrush.

The pressure sensitive layer was modeled as a mass-spring system to determine the actual pressure induced on the sensor. Through several simulated results, resistance variation limits of FSR as well as the voltage ranges were determined. Based on a logic table, the circuit schematic was designed and simulated by using the MATLAB Simulink block diagram. Satisfactory results led to an experimental setup, testing, and finally to prototype development. The results of the experiment were quite impressive and proved the viability of the proposed system for practical applications. The presented system is an experimental prototype and must go through a proper manufacturing process before it can be tested with real subjects. The integration of Internet of Things will upgrade the proposed system to the next level.

Peer-review: Externally peer-reviewed.

Acknowledgements: The author would like to express his gratitude to the Ministry of Education, Bangladesh; Department of CSE, Military Institute of Science and Technology (MIST), Dhaka, Bangladesh; and R&D (Robotics) section of DREAM Robotics Ltd., Dhaka, Bangladesh. The author is also thankful to the editors and anonymous reviewers for providing insightful suggestions and comments to improve the quality of this paper.

Conflict of Interest: The authors have no conflicts of interest to declare.

Financial Disclosure: The authors declared that this study has received no financial support.

References

1. M. Wolf, P. Klein, R. Engelmohr, J. Erb, "Data on toothbrushing study comparing infrared-based motion tracking versus video observation", Data in Brief, Elsevier, vol. 13, pp. 1-5, 2020. [Crossref]
2. M. Akhtaruzzaman, "Prototype of a force-sensitive smart toothbrush", In Proc. EICT, 4th Int. Conf., 2019.
3. STATISTA, Usage of manual toothbrushes in the u.s. 2019. URL: https://www.statista.com/statistics/278116/us-households-usage -of-manual-toothbrushes.
4. STATISTA, Usage of manual toothbrushes in the u.s. 2011-2023. URL: https://www.statista.com/statistics/287357/usage-of-manual-toothbrushes-in-the-us-trend.
5. STATISTA, Toothbrushes usage in great britain 2015-2018, by type. URL: https://www.statista.com/statistics/303553/toothbrushe-susage-by-type-in-the-uk.
6. STATISTA, Type of toothbrush used to brush teeth in the United Kingdom 2016. URL: https://www.statista.com/statistics/549289 / toothbrush-used-to-brush-teeth-in-the-united-kingdom-uk.
7. Electric toothbrushes thrive in developed markets. URL: https://blog.euromonitor.com/electric-toothbrushes-thrive-in-developed-markets/.
8. S. Z. Mostarin, P. Khyang, S.R. Roy, "Dental health care in bangladesh: Prospects and challenges", Discovery Publication, vol. 55 no. 280, pp. 137-141, 2019.
9. I. Digel, I. Kern, E. M. Geenen, N. Akimbekov, "Dental plaque removal by ultrasonic toothbrushes", Dentistr J, vol. 8, no.1, pp. 28, 2020. [Crossref]
10. P. Bottenberg, H. Verhelle, A. D. Bruyne, C. Vercruysse, M. Buijs, "Fluoride concentration in saliva after toothbrushing with electrical and manual toothbrush", In: 66th ORCA Congress, Cartagena, Colombia, pp. 394, 2019.
11. C. Ng, J. K. H. Tsoi, E. C. M. Lo, J. P. Matinlinna, "Safety and design aspects of powered toothbrush - a narrative review", Dentistr J, vol. 8, no. 1, pp. 15, 2020. [Crossref]
12. N.C. Sharma, M. Klukowska, A. Mielczarek, J.M. Grender, J. Qaqish, "A 4-week clinical comparison of a novel multi-directinal power brush to a manual toothbrush in the reduction of gingivitis and plaque", Am J Dentistry, vol. 25, pp. 16-22, 2012.
13. L. R. E. Gonzales, K. D. G. Latoza, E. M. P. Fabian, C. D. Danganan, M. C. L. Yambao, S. Wong, "A comparative study on surface changes between composite veneer and acrylic resin using battery-operated toothbrush and manual toothbrush", in: Asia Proceedings of Social Sciences 5(1), 5th ASIA International Conference, KLCC, Malaysia, pp. 29-32, 2012. [Crossref]
14. M. Akhtaruzzaman, A. A. Shafie, "A novel gait for toddler biped and its control using pic 16f877a", In: Proceedings of 2011 4th International Conference on Mechatronics (ICOM '11), Kuala Lumpur, Malaysia, 2011. [Crossref]
15. M. Akhtaruzzaman, A.A. Shafie, M.R. Khan, "Electro-goniometric system; an instrumentation to capture knee movements for forward walking", In: The 10th Asian Control Conf. (ASCC), Sabah, Malaysia, 2015. [Crossref]
16. M. H. Masud, M. Akhtaruzzaman, S. M. S. Bari, F. Anwar, "Engineers' obligations towards sustainable environment", In: 2nd International Conference on Professional Ethics and Education in Engineering (ICEPEE), Kuala Lumpur, Malaysia, pp. 85-92, 2011.
17. D. Giuliani, W. McMahon, J. C. McInnes, "Toothbrush with adaptive load sensor", United States Patent, 5748742.
18. A. H. Slocum, J. T. Slocum, "Force sensitive toothbrush, United States Ptent Application Publication", No. US 2014/0020198 A1.
19. M. Bizhang, K. Riemer, W. H. Arnold, J. Domin, S. Zimmer, "Influence of bristle stiffness of manual toothbrushes on eroded and sound human dentin - an in vitro study", PLoS One vol. 11, no. 4, pp. e0153250, 2016. [Crossref]
20. A. Matsumoto, Y. Musha, "Tooth brushing pressure indicator", Google Patents, JPH10108734A.
21. R. S. Dirksing, "Force-indicating toothbrush using magnetic latching", United States Patent, No. 5355544.
22. E. L. Spieler, R. M. Berman, "Force sensitive handle for hand operated implement", United States Patent, No. 5282291.
23. Y. Chiyoda, "Toothbrush with polishing pressure sensor", Google Patents, JPH07236519A.
24. K. A. Miller, "Resonantly driven power toothbrush having a pressuresensing capability using a hall effect sensor", United States Patent Application Publication, No. US 2015/0230898 A1.
25. 3m vhb double coated acrylic foamtapes and adhesives transfer tapes, technical data (2001). URL: http://www.puiaudio.com/p df/ Exciter/3MVHBDatasheet.pdf.
26. 3m vhb tape, technical data (2011). URL: https://www.alliedelec.com/m/d/e4e1ef3b96100de3bc461d617b0cdfa2.pdf.

27. R. Thevamaran, F. Fraternali, C. Daraio, "Multiscale mass-spring model for high-rate compression of vertically aligned carbon nanotube foams", J Appl Mech, vol. 81, no. 12, pp. 121006-1, 2014. [Crossref]
28. J. V. Mane, S. Chandra, S. Sharma, H. Ali, V. M. Chavan, B. S. Manjunath, R. J. Patel, "Mechanical property evaluation of polyurethane foam under quasi-static and dynamic strain rates- an experimental study", Procedia Engineering, vol. 173, pp. 726-731, 2017. [Crossref]
29. V. Goga, B. Hučko, "Phenomenological material model of foam solids", Journal of Mechanical Engineering - Strojnícky časopis, vol. 65, no. 1, pp. 5-20, 2015. [Crossref]
30. Interlink electronics, fsr® force sensing resistors®, fsr® integration guide (2020). URL: file:///C:/Users/USER/AppDat a/Local/Temp/interlink-electronics-fsr-force-sensing-resistors-int egration-guide.pdf.
31. D. Zenkert, M. Burman, "Tension, compression and shear fatigue of a closed cell polymer foam", Composites Science and Technology, vol. 69, no. 6, pp. 785-792, 2009. [Crossref]



Dr. M. Akhtaruzzaman received the B. Sc. degree in computer science and engineering (CSE) from International Islamic University Chittagong (IIUC), Bangladesh in 2005. He received the M. Sc. degree in mechatronics engineering (MCT) from Kulliyyah of Engineering, International Islamic University Malaysia (IIUM), Malaysia in 2012. He was awarded a Ph. D. degree in Engineering (Mechatronics & Robotics) from Kulliyyah of Engineering, IIUM, Malaysia

Dr. Akhtaruzzaman is an Assistant Professor in the department of Computer Science and Engineering (CSE), Military Institute of Science and Technology (MIST), Dhaka, Bangladesh. He is associated with one of the prominent journals in Bangladesh, MIST International Journal of Science and Technology (MIJST); and with DREAM Robotics Ltd., Dhaka, Bangladesh as a Consultant and Research scientist. He has published several research articles including journals, conferences, books, and book chapters in the area of modeling and control, robotics, mechatronics system design, and machine intelligence. His research interests include modeling and control of mechatronics systems, robotics, rehabilitation engineering, computational musicology, algorithm design, and AI.